China Geology 2 (2021) 215−229

China Geology

Journal homepage: http://chinageology.cgs.cn
https://www.sciencedirect.com/journal/china-geology

Archean (about 2500 Ma) anatexis in eastern North China Block

Si-hong Jiang[a,*], Leon Bagas[a, b], Yi-fei Liu[a], Li-li Zhang[a]

[a] *Ministry of Natural Resources Key Laboratory of Metallogeny and Mineral Assessment, Institute of Mineral Resources, Chinese Academy of Geological Sciences, Beijing* 100037, *China*
[b] *Centre for Exploration Targeting, The University of Western Australia, Crawley, WA* 6009, *Australia*

ARTICLE INFO

Article history:
Received 5 May 2020
Received in revised form 14 July 2020
Accepted 27 October 2020
Available online 3 March 2021

Keywords:
Neoarchean granodioritic orthogneiss
Granulite-facies
Neoarchean granite
Isotope disequilibrium
Geological survey engineering
North China Block

ABSTRACT

Two Neoarchean alkaline feldspar-rich granites sourced from partially melted granulite-facies granodioritic orthogneiss have been here recognised in the eastern part of the North China Block (NCB). These poorly foliated granites have previously been assumed to be Mesozoic in age and never dated, and so their significance has not been recognised until now. The first granite (AG1) is a porphyritic syenogranite with megacrystic K-feldspar, and the second (AG2) is a quartz syenite with perthitic megacryst. Zircons from the granites yield LA-ICP-MS U-Pb ages of 2499 ± 10 Ma (AG1), and 2492 ± 28 Ma (AG2), which are slightly younger than the granodioritic orthogneiss that they intrude with a crystallisation U-Pb age of 2537 ± 34 Ma. The younger granites have higher assays for SiO_2 (71.91% for AG1 and 73.22% for AG2) and K_2O (7.52% for AG1 and 8.37% for AG2), and much lower assays for their other major element than the granodioritic orthogneiss. All of the granodioritic orthogneiss and granite samples have similar trace element patterns, with depletion in Th, U, Nb, and Ti and enrichment in Rb, Ba, K, La, Ce, and P. This indicates that the granites are derived from the orthogneiss as partial melts. Although they exhibit a similar REE pattern, the granites have much lower total REE contents (30.97×10^{-6} for AG1, and 25.93×10^{-6} for AG2), but pronounced positive Eu anomalies (Eu/Eu* = 8.57 for AG1 and 27.04 for AG2). The granodioritic orthogneiss has an initial $^{87}Sr/^{86}Sr$ ratio of 0.70144, $\varepsilon Nd(t)$ value of 3.5, and $\varepsilon Hf(t)$ values ranging from −3.2 to +2.9. The orthogneiss is a product of fractional crystallisation from a dioritic magma, which was derived from a mantle source contaminated by melts derived from a felsic slab. By contrast, the AG1 sample has an initial $^{87}Sr/^{86}Sr$ ratio of 0.6926 that is considered too low in value, $\varepsilon Nd(t)$ value of 0.3, and $\varepsilon Hf(t)$ values between +0.57 and +3.82; whereas the AG2 sample has an initial $^{87}Sr/^{86}Sr$ ratio of 0.70152, $\varepsilon Nd(t)$ value of 1.3, and $\varepsilon Hf(t)$ values between +0.5 and +14.08. These assays indicate that a Sr-Nd-Hf isotopic disequilibrium exists between the granite and granodioritic orthogneiss. The elevated $\varepsilon Hf(t)$ values of the granites can be explained by the involvement of Hf-bearing minerals, such as orthopyroxene, amphibole, and biotite, in anatectic reactions in the granodioritic orthogneiss. Based on the transitional relationship between the granites and granodioritic orthogneiss and the geochemical characteristics mentioned above, it is concluded that the granites are the product of rapid partial-melting of the granodioritic orthogneiss after granulite-facies metamorphism, and their crystallisation age of about 2500 Ma provides the minimum age of the metamorphism. This about 2500 Ma tectonic-metamorphic event in NCB is similar to the other cratons in India, Antarctica, northern and southern Australia, indicating a possible connection between these cratons during the Neoarchean.

1. Introduction

Anatexis takes place in high-grade metamorphic terranes and orogens (Liu FL et al., 2009; Liu R et al., 2010; Vanderhaeghe O, 2009; Carvalho BB et al., 2017; Dong C et al., 2017; Rocha BC et al., 2017; Liu F et al., 2019). Many experiments and experimental simulations have been performed synthesizing partial melting employing the dehydration-melting model (London D et al., 2012; Aranovich LY et al., 2014; Newton RC et al., 2014). Dehydration melting involves the breakdown of hydroxide-bearing phases to produce a water-undersaturated melt and anhydrous solids (Burnham CW, 1967; Clemens JD, 1984; Grant JA, 1985; Vielzeuf D and Schmidt MW, 2001).

Generally, there are two types of anatexis, one is fluid-present partial melting and the other fluid-absent partial

* Corresponding author: *E-mail address*: jiangsihong1@163.com (Si-hong Jiang).

doi:10.31035/cg2021014
2096-5192/© 2021 China Geology Editorial Office.

melting, which are discussed in detail by Stevens G and Clemens JD (1993) and Clemens JD and Droop GTR (1998). Fluid-present melting takes place at or near the solidus involving quartz and feldspar. Given that a small amount of free water can be stored along mineral boundaries, fluid-present melting produces very low amounts (<1 vol.%) of a melt, unless external water is added to the system (Kriegsman LM, 2001). By contrast, fluid-absent partial melting forms far above the solidus and involves the breakdown of hydrous minerals (such as mica and amphibole). As the resultant melts are generally H_2O-poor (undersaturated) and the amount of H_2O available for melting in hydrous minerals is significant (2 vol.% –5 vol.%), the volume of melt produced reaches values of up to 30 vol.%, depending on the melt fertility of the rocks, which far exceeds the amount in fluid-present melting (Clemens JD, 1984; Clemens JD and Vielzeuf D, 1987; Kriegsman LM, 2001).

Other factors may affect partial melting as discussed by Aranovich LY et al. (2014) who suggest that the volatile components CO_2 and Cl are important agents in deep-crustal metamorphism and anatexis. Stevens G et al. (1997) conducted fluid-absent partial melting experiments at pressures of 0.5 GPa and 1 GPa and temperatures between 750℃ and 1000℃, investigating the influence of bulk-rock Mg# [100Mg/(Mg+Fe)] and the effects of additional TiO_2 on granulite-grade anatectic evolution of relatively magnesian-rich metamorphosed shale and greywacke. It was found that melting began between 780℃ and 830℃ with the breakdown of biotite and production of quartz-saturated granulite-facies residual mineral assemblages. It was also found that the mineral assemblages were in equilibrium with H_2O-undersaturated granitic melt.

Also, element and isotope disequilibrium during crustal anatexis are documented (Farina F et al., 2014; Chen YX et al., 2015; Carvalho BB et al., 2017; Gardiner NJ et al., 2017; Huang H et al., 2017). For example, Ayres M and Harris N (1997) document REE fractionation and Nd-isotope disequilibrium of Himalayan leucogranites during crustal anatexis. Davies GR and Tommasini S (2000) propose that rapid crustal anatexis will produce a sequence of chemically and isotopically distinct melts that are in isotopic disequilibrium with their crustal source.

Although anatexis and migmatisation have been described in other parts of the North China Block (NCB; Ren LD et al., 2011; Dong C et al., 2017; Liu F et al., 2019), they are less studied in Eastern Hebei Province, which is one of the best-exposed areas for the Archean metamorphic rocks in northern China. Eastern Hebei Province is accessible and close to Beijing, with the presence of about 3860 Ma detrital zircons from fuchsite quartzite in the Caozhuang Complex (Liu DY et al., 1992; Liu SJ et al., 2013; Wilde SA et al., 2008). These zircons must have been derived from units of this age, which might be present at depth in the complex, or are allochthonous. This makes the region a natural laboratory for the study of the evolution of Archean rocks and has attracted many geoscientists (Nutman AP et al., 2011; Zhang LC et al., 2012; Guo RR et al., 2015; Li LX et al., 2015; Bai X et al., 2016; Kwan LCJ et al., 2016; Yang C and Wei C, 2017; Duan Z et al., 2017, 2019; Fu J et al., 2017; Liou P et al., 2019).

The age of metamorphic rocks and their magmatic precursors in Eastern Hebei Province are documented, and the tectonic settings have been discussed by previous authors (Wilde SA et al., 2008; Guo RR et al., 2015; Bai X et al., 2016; Li LX et al., 2015; Duan Z et al., 2017, 2019; Fu J et al., 2017; Liou P et al., 2019; Geng YS et al., 2018; Wan YS et al., 2018). The magmatic precursors of orthogneiss record a about 2900 Ma magmatic event at the Caochang Village in the region (Fig. 1b; Liou P et al., 2019). Metavolcanic rocks in the Saheqiao area are N-MORB-like basaltic rocks, primitive arc basaltic rocks, island arc-like rocks, and Nb-enriched basalt (NEB)-like rocks, with magmatic crystallisation ages of 2614–2518 Ma, indicative of an arc-related tectonic setting (Guo RR et al., 2013). In contrast, metavolcanic rocks in the Qinglong-Zhuzhangzi area include depleted low Ti tholeiite, primitive and evolved arc tholeiite, and K-rich andesite-dacite interpreted as a complete subduction cycle ranging from orogen to primitive arc-evolved arc and back to an orogenic setting during the period 2604 Ma to 2511 Ma (Guo RR et al., 2015). Additionally, Li LX et al. (2015) document the presence of 2545 Ma and 2523 Ma banded iron-formation (BIF) in the area, which they propose was deposited in an arc-related basin.

Neoarchean orthogneiss from the Zunhua-Qinglong area consists of schlieric dioritic to tonalitic orthogneiss, monzogranitic orthogneiss, charnockitic plagioclase orthogneiss, and charnockite (Bai X et al., 2014, 2015; Guo RR et al., 2013, 2015). Protoliths of dioritic-trondhjemitic orthogneiss in the northern Zunhua area have interpreted crystallisation ages of 2535 –2513 Ma, with suggested magmatic sources including depleted mantle and subducted slab melts related to a Neoarchean subduction-related tectonic setting (Bai X et al., 2014). Bai X et al. (2015) also document the presence of charnockite in the Taipingzhai-Yuhuzhai and Cuizhangzi areas contain magmatic orthopyroxene crystallised directly from their magmatic precursors. They propose that the magmatic precursors are sourced from a subducted and partially melted slab strongly contaminated by 2527–2515 Ma mantle peridotite. LA-ICP-MS zircon U-Pb isotopic dating reveals that the magmatic precursors of these monzogranitic and syenogranitic orthogneisses in the southern part of the Eastern Hebei and Western Liaoning provinces were emplaced during 2527–2511 Ma interpreted in a back-arc basin setting (Fu J et al., 2017, and references therein). These studies propose the presence of a subduction zone dipping southeast along the northern part of eastern NCB (Bai X et al., 2016). The Neoarchean geodynamic evolution in Eastern Hebei Province, however, is still uncertain. In contrast to the subduction-related model, it is proposed that a Neoarchean mantle plume led to widespread magmatism and metamorphism, during a restricted period between about 2550 Ma and 2500 Ma (Geng YS et al., 2006, 2016; Yang JH et al., 2008; Zhao GC et al., 1998, 1999).

The *P-T* path of the metamorphism has also been studied using conventional thermobarometers with peak *P-T* conditions for mafic granulite estimated to be 900–1100 MPa at temperatures between 810℃ and 940℃, 950 MPa at 780–816℃, and 800–850 MPa at 850–900℃ (He GP and Ye HW, 1992; Chen MY and Li SX, 1996; Zhao GC et al.,

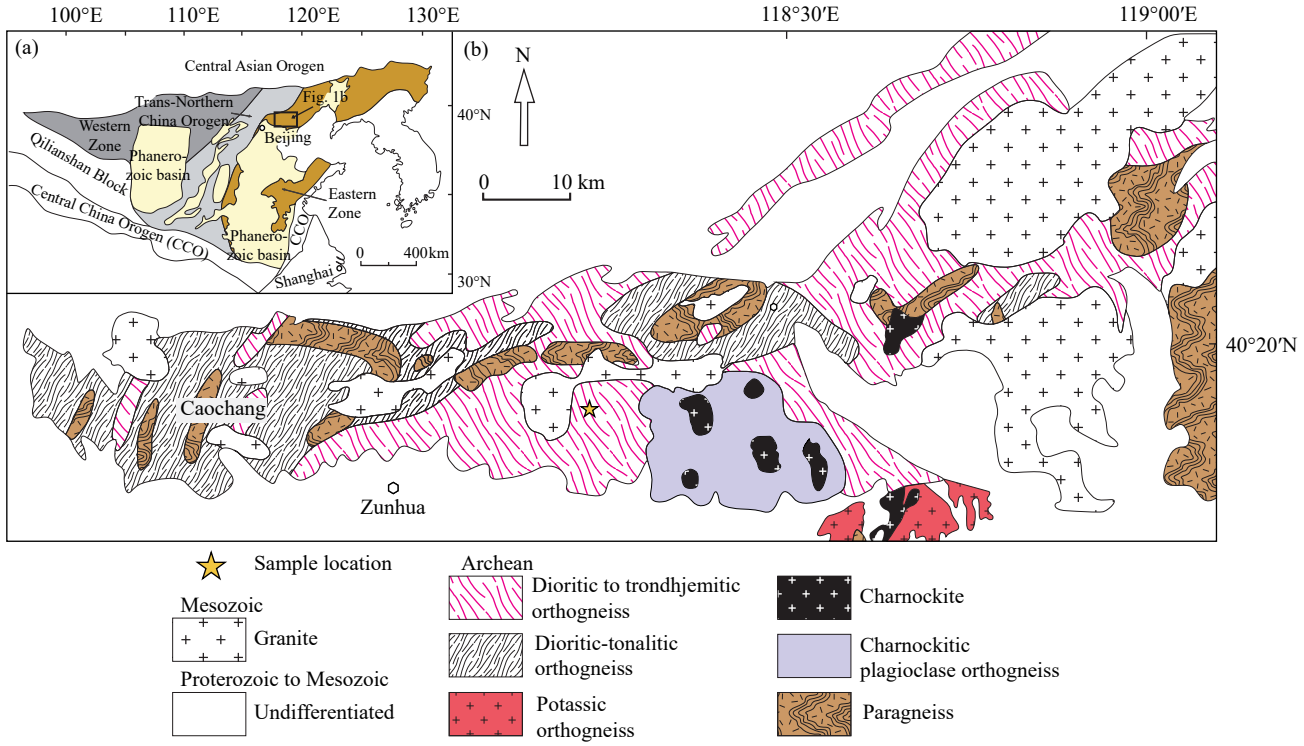

Fig. 1. Geological map showing: a–tectonic units of the NCB and location of the study area (modified from Zhao GC et al., 2005); b–geological sketch map of the Malanyu Antiform in Eastern Hebei Province showing the locations of the samples for which U-Pb and Lu-Hf zircon analyses were completed (modified from Bai X et al., 2016 and Geological Survey of Hebei Province, 1970).

1998). Recently, mafic granulite and charnockite located at Taipingzhai were estimated using pseudo section modelling with THERMOCALC, giving a 960–1030 MPa pressure at temperatures between 860℃ and 900℃ and 700–1400 MPa at 800–920℃ (Kwan LCJ et al., 2016; Yang QY et al., 2016). The same method has been employed for Archean pelitic granulite from the Taipingzhai and Laolijia areas in Eastern Hebei Province, which record an anticlockwise *P-T* path with the peak metamorphism at a temperature of >950℃ and pressure of 900 MPa (Duan Z et al., 2017). As can be seen, these estimated *P-T* values are very similar obtained using different methods.

Anatectic potassic granitic veins are thought to be rare in Eastern Hebei Province (He GP and Ye HW, 1992; Lin Q et al., 1992). Nutman AP et al. (2011) report a zircon U-Pb age of 2503 ± 11 Ma for a pegmatite with orthopyroxene megacrysts intruding leptynite in the area. Li LX et al. (2015) propose that the anatectic event in the region extended from 2511 Ma to 2485 Ma, based on U-Pb dating of zircon grains with light-grey tones on their rims using cathodoluminescence (CL) images and newly grown homogeneous grains from the migmatitic rocks peaking at 2506 Ma, immediately following deposition of BIF.

Although the ages of the pegmatite and development of migmatite related to the granulite-facies metamorphism in Eastern Hebei Province have been studied, Neoarchean granites formed from partial melting of granulite-facies orthogneiss have not been reported. In this contribution, the authors present new zircon LA-ICP-MS U-Pb dates, whole-rock geochemistry, Sr-Nd isotopic geochemistry, and zircon Hf isotopic data for granites hosted by and sourced from granodioritic orthogneiss during partial melting. The aims of this study are: (1) Constrain the timing of the anatexis; (2) trace the elements and isotope behaviour during anatexis; (3) discuss the relationship between the granulite-facies metamorphism and Neoarchean granitic intrusions.

2. Geological setting

The NCB is bound by the Early Paleozoic to Early Mesozoic Central Asian Orogen to the north and Qinling-Dabie-Sulu Orogen to the south (Fig. 1a). The block is commonly and broadly subdivided into the Archean Eastern and Western zones separated by the Paleoproterozoic Trans-Northern China Orogen (Zhao GC et al., 2001). Most of the Archean rocks are Neoarchean, and older (possibly Eoarchean) rocks are in the northeastern part of the Eastern Zone (Liu DY et al., 1992; Liu ZH and Yang ZS, 1994; Wilde SA et al., 2008). The Archean rocks are multiply deformed, and metamorphosed to granulite facies (Zhai MG and Santosh M, 2011). Previous authors have dated the metamorphism between about 2500 Ma and 2370 Ma with a peak at about 2450 Ma (Bai X et al., 2016, 2014; Guo RR et al., 2013).

The Malanyu Antiform is an example of multiply folded and faulted structure located northeast of Beijing (Figs. 1a, b). The antiform is doubly plunging, trends eastward, and its Archean core (inlier) is around 110 km long and 30 km wide. The Archean to Early Paleoproterozoic rocks include orthogneiss, gneisses derived from supercrustal rocks. The supercrustal gneisses appear to form rafts within the orthogneiss, or the orthogneiss was originally a lopolith within the paragneiss and the present distribution of the

paragneiss is controlled by interference folding (Fig. 1b). The composition of the orthogneiss in the western part of the antiform is dioritic to tonalitic, in the east is dioritic, tonalitic, trondhjemitic, granodioritic, and monzogranitic, and the south-central part of the antiform includes minor charnockitic plagioclase-rich orthogneiss and charnockite.

The gneisses in the Malanyu Antiform are unconformably overlain by Late Paleo- to Neoproterozoic sequences consisting of quartz sandstone, siltstone, mudstone, dolomite and rare pyroclastic (tuffaceous) units, and an Early Paleozoic sequence of carbonate rocks, and Mesozoic volcanic-sedimentary rocks (Fig. 1b).

At least three major deformation events are affecting the Late Paleo- to Neoproterozoic sedimentary and rare volcanic units in the area represented by folds orientated 110°–290° (F_1), 60°–240° (F_2), and 20°–200° (F_3) (Jiang SH et al., 2018). These structures relate to compression orientated 20°–200° (D_1), 150°–330° (D_2) and 110°–190° (D_3) (Jiang SH et al., 2018).

Mesozoic granites are concentrated in the Archean rocks along the axis of the Malanyu Antiform, although rare Mesozoic granites intrude the synclinal folded Proterozoic rocks to the north of the antiform's core (Fig. 1b). These intrusives consist of quartz monzonite, syenogranite, granodiorite, and monzogranite, and commonly have ellipsoidal shape rafts (or windows) with long axes trending subparallel to the axis of the antiform (Jiang SH et al., 2018).

3. Sample description and analytical methods

3.1. Description of orthogneiss and granite samples

Three samples were collected from near an open-cut iron-ore mine located in the Archean Malanyu Inlier (Fig. 1b).

Sample JD16-049 is a granodioritic orthogneiss from 40°15′09″N and 118°13′42″E (Fig. 2a), with the foliation dipping 85ºS, and consists of pyroxene (about 15 vol.%), amphibole (about 5 vol.%), biotite (about 15 vol.%), plagioclase (about 50 vol.%), and quartz (about 15 vol.%; Fig. 2d).

Sample JD16-50 is light red syenogranite (AG1) from 40°15′09″N and 118°13′42″E, where it intrudes the granodioritic orthogneiss and contains xenoliths of the orthogneiss. The syenogranite consists of megacrysts K-feldspar (about 65 vol.%), fine-grained quartz (about 20 vol.%), and plagioclase (about 15 vol.%; Fig. 2e, f).

Sample JD16-052 is a quartz syenite (AG2) from 40°14′55″E and 118°13′51″N (Fig. 2c), which has a gradational contact with the granodioritic orthogneiss. The sample consists of perthite (about 35 vol.%), megacrysts K-feldspar (35 vol.%), fine-grained quartz (15 vol.%), and plagioclase (15 vol.%; Fig. 2g, h). Mafic minerals, such as hornblende and biotite are rare in both AG1 and AG2 and form lensoidal dykes interpreted as the product of the in situ anatexis in the granodioritic orthogneiss (Fig. 2a).

3.2. Analytical methods

3.2.1. LA- ICP-MS U-Pb zircon dating

Three samples were collected from the granodioritic orthogneiss and granites for Laser Ablation Inductively Coupled Plasma Mass Spectrometry (LA-ICP-MS) U-Pb zircon dating. The samples were crushed, sieved and the heavy mineral fraction was separated using magnetic and heavy liquid separation methods to concentrate zircons. The zircons were then handpicked, placed in standard GJ-1 epoxy resin mounts, and polished. The binocular microscope and cathodoluminescence (CL) imaging were used to study the morphology and internal structure of the zircons before the grains were selected for U-Pb isotope analyses. CL images were produced using a JSM-6510 with a GATAN MiniCL detector at Beijing Createch Testing Technology Co. Ltd. All U-Pb dating analyses were completed using a LA-ICP-MS at Beijing Createch Testing Technology Co. Ltd. Detailed operating conditions for the laser ablation and ICP-MS instruments and data reduction are the same as a description by Hou KJ et al. (2009). Laser ablation was performed using an ESI NWR 193 nm laser ablation platform, and ion-signal intensities were measured using an AnlyitikJena PQMS Elite ICP-MS instrument. Helium was used as a carrier gas, and argon was used as the make-up gas mixed with the helium in a T-connector before entering the ICP. Each analysis included a background acquisition of approximately 15 s (gas blank) followed by 45 s data acquisition from the sample. Off-line raw data selection and integration of background and analysed signals, and time-drift correction and quantitative calibration for U-Pb dating was calculated using the ICPMSDataCal software (Liu YS et al., 2010).

The GJ1 zircon was used as an external standard and was analysed twice every five analyses. Time-dependent drifts of U-Th-Pb isotopic ratios were corrected using linear interpolation with time for every ten analyses according to the variations of GJ1 (i.e. 2 zircon GJ1 + 10 samples + 2 zircon GJ1) (Liu YS et al., 2010). The preferred U-Th-Pb isotopic ratios used for the zircon GJ1 standard are documented by Jackson SE et al. (2004) and preferred the uncertainty of the value of <0.5% for GJ1 was propagated to the analyses of the dated samples. Common Pb correction was not necessary because of the low signal of common ^{204}Pb and high $^{206}Pb/^{204}Pb$ ratio of the samples dated. The U, Th, and Pb concentrations were calibrated using the NIST 610 glass standard. Concordia diagrams and weighted mean calculations were made using the Isoplot/Ex_ver3 program of Ludwig KR (2003). The standard Plesovice zircon is dated as an unknown sample yield weighted mean $^{206}Pb/^{238}U$ age of 337 ± 2 Ma (2σ, n = 30), which is in good agreement with the recommended $^{206}Pb/^{238}U$ age of 337.13 ± 0.37 Ma (2σ) (Sláma J et al., 2008).

3.2.2. Major and trace element analyses

Whole-rock analyses were completed in the Analytical Center at the Beijing Institute of Geology for Nuclear Industry (ACBIGNI). Major element compositions were determined with X-ray fluorescence (Philip PW2404) using fused disks. Trace elements were determined using an ICP-MS (Finnigan-MAT Element I) after acid digestion of samples in Teflon bombs. The analytical precision and accuracy of the analyses are better than 5% for major elements and 10% for trace

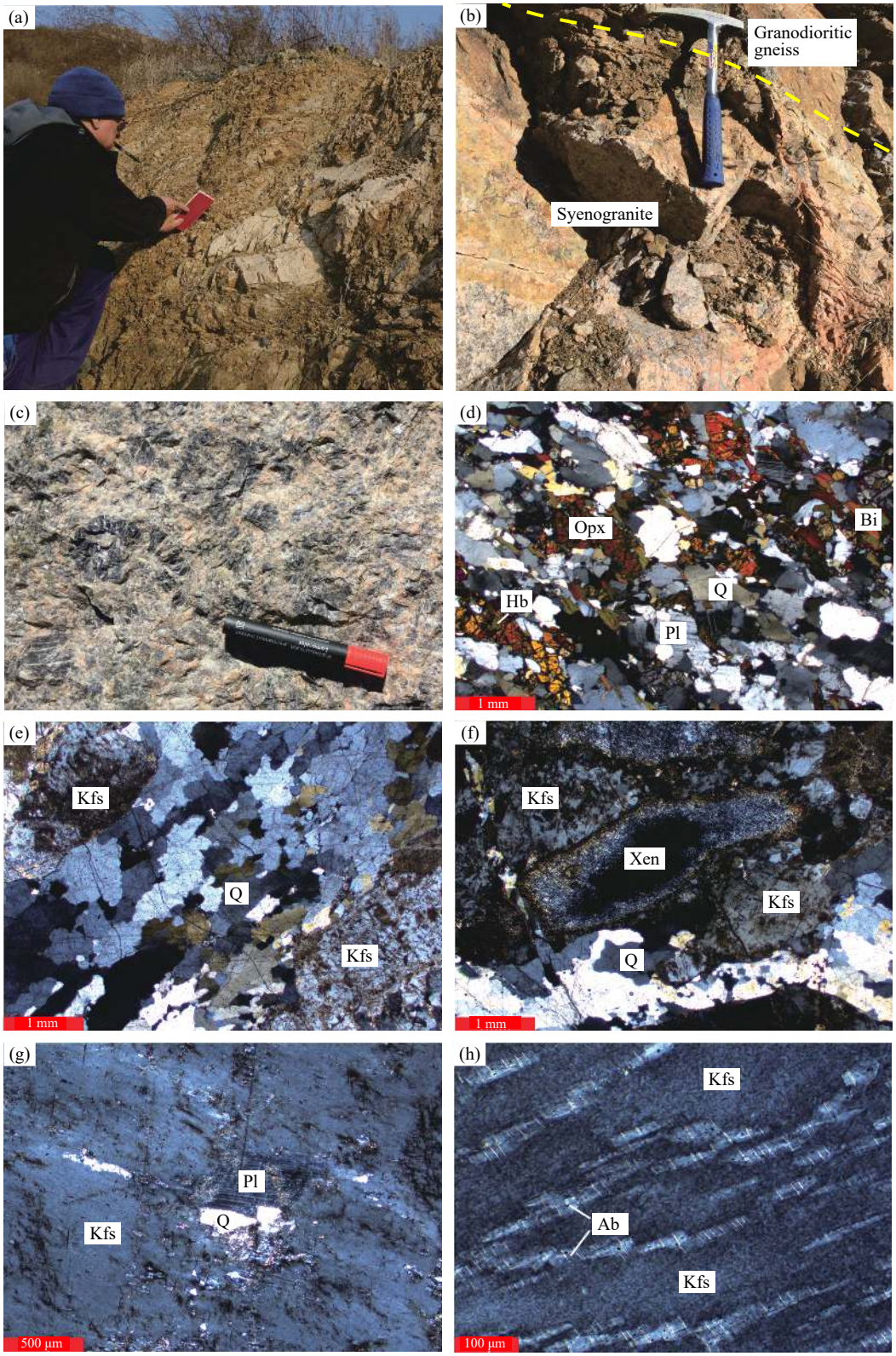

Fig. 2. Photographs and photomicrographs of granodioritic orthogneiss, syenogranite, and quartz syenite from the Archean Malanyu Inlier. a–granodioritic orthogneiss with moderate foliation and intruded lensoidal syenogranite dykes; b–light red anatectic granite (AG1) showing transitional relationships with granodioritic orthogneiss; c–anatectic granite (AG2) with dark perthitic megacryst; d–medium-grained granodioritic orthogneiss sample JD16-049 consisting of aligned orthopyroxene, hornblende, biotite, plagioclase, and quartz; e–syenogranite (AG1) sample JD16-050 with K-feldspar megacryst and veinlet-like quartz; f–xenolith of the host granodioritic orthogneiss within syenogranite (AG1); g–quartz syenite (AG2) sample JD16-052 with K-feldspar megacryst and fine-grained quartz and plagioclase. The polysynthetic twinning can still be seen in plagioclase; h–quartz syenite (AG2) sample JD16-052 with small albite crystals in perthitic feldspar. Ab-albite; Hb–hornblende; Bi–biotite; Opx–orthopyroxene; Kfs–K-feldspar, Pl–plagioclase; Q–quartz; Xen-xenolith. All the photomicrographs are taken under cross-polarized light. The hammer and marker pen in the photographs are 410 mm and 140 mm long, respectively.

elements.

Sample JD16-049 plots in the granodiorite field in the An-Ab-Or diagram (not shown; Barker F, 1979).

3.2.3. Rb-Sr and Sm-Nd isotope analyses

Whole-rock Rb-Sr and Sm-Nd isotopic ratios were determined on an ISOPROBE-T at ACBIGNI. The $^{147}Sm/^{144}Nd$ and $^{87}Rb/^{86}Sr$ ratios were calculated using Sm, Nd, Rb, and Sr concentrations measured with an ICP-MS. The measured $^{143}Nd/^{144}Nd$ were normalised to $^{146}Nd/^{144}Nd$ = 0.7219, and $^{87}Sr/^{86}Sr$ ratios to $^{86}Sr/^{88}Sr$ = 0.1194. The SHINESTU Nd standard was measured during analyses yielding a $^{143}Nd/^{144}Nd$ ratio of 0.512118 ± 3 (2σ), and the NBS-987 Sr standard yielded a $^{87}Sr/^{86}Sr$ ratio of 0.71025 ± 7 (2σ).

3.2.4. In-situ zircon Hf isotopic analysis

In-situ zircon Hf isotope analysis was completed on dated spots using an ESI NWR193 laser-ablation microprobe, which was attached to a Neptune plus multi-collector ICP-MS at the Beijing CreaTech Testing International Co. Ltd. Instrumental conditions and data acquisition are comprehensively described by Wu FY et al. (2006) and Hou KJ et al. (2007). A stationary spot was used for the present analyses, with a beam diameter of 40 μm depending on the size of ablated domains. Helium was used as a carrier gas to transport the ablated sample from the laser-ablation cell to the ICP-MS torch via a mixing chamber mixed with Argon. The $^{176}Lu/^{175}Lu$ = 0.02658 and $^{176}Yb/^{173}Yb$ =0.796218 ratios were determined to correct the isobaric interferences of ^{176}Lu and ^{176}Yb on ^{176}Hf (Chu NC et al., 2002). For instrumental mass bias correction, the $^{172}Yb/^{173}Yb$ ratios were normalised to 1.35274 (Chu NC et al., 2002) and the $^{179}Hf/^{177}Hf$ ratios to 0.7325 using an exponential law. The mass bias behaviour of Lu was assumed to follow that of Yb, and the mass bias correction protocol details were described by Wu FY et al. (2006) and Hou KJ et al. (2007). The zircon GJ1 standard was used as the reference standard during the routine analyses, with a weighted mean $^{176}Hf/^{177}Hf$ ratio of 0.282007 ± 0.000007 (2σ, n=36). This value is not distinguishable from a weighted mean $^{176}Hf/^{177}Hf$ ratio of 0.282000 ± 0.000005 (2σ) using a solution analysis method by alysis method by Morel MLA et al. (2008). Single zircon U-Pb ages were used to calculate $\varepsilon Hf(t)$ values adopting the present-day chondritic ratios of $^{176}Hf/^{177}Hf$ = 0.282772 and $^{176}Lu/^{177}Hf$ = 0.0332 (Blichert-Toft J and Albarède F, 1997). Single-stage model ages (t_{DM1}) were calculated by referring to a depleted mantle with a present-day $^{176}Hf/^{177}Hf$ ratio of 0.28325 and $^{176}Lu/^{177}Hf$ ratio of 0.0384 (Vervoort JD and Blichert-Toft J, 1999). Two-stage model ages were calculated with an assumed $^{176}Lu/^{177}Hf$ ratio of 0.015 for the average continental crust (t_{DM2}; Griffin WL et al., 2002).

4. Results

4.1. U-Pb zircon geochronology

Twenty LA-ICP-MS U-Pb analyses were completed on 20 zircons from the granodioritic orthogneiss (sample JD16-049). The zircons have short prismatic shapes, with length/width ratios between 1∶1 and 2∶1. The CL images show that the zircons contain distinct cores with a blurry oscillatory zonation and bright structureless rims (e.g. spots 1, 4, 7, and 9; Fig. 3a). Spot 4 located at the core of zircon with oscillatory zonation has the oldest $^{207}Pb/^{206}Pb$ date of 3059 ± 17 Ma and a Th/U value is 0.26, which is interpreted as being xenocrystic (Fig. 3a; Appendix Table S1). The second oldest $^{207}Pb/^{206}Pb$ date of 2639 ± 17 Ma is from spot 9 located on a dark sector of a rounded zircon with a Th/U value of 0.76 and is interpreted as being xenocrystic. Except for spot 19, which is not included in the age calculation due to its large error and low concordance, the other 17 analyses include 14 located on blurry oscillatory-zoned inner cores (e.g. spot 1 in Fig. 3) and

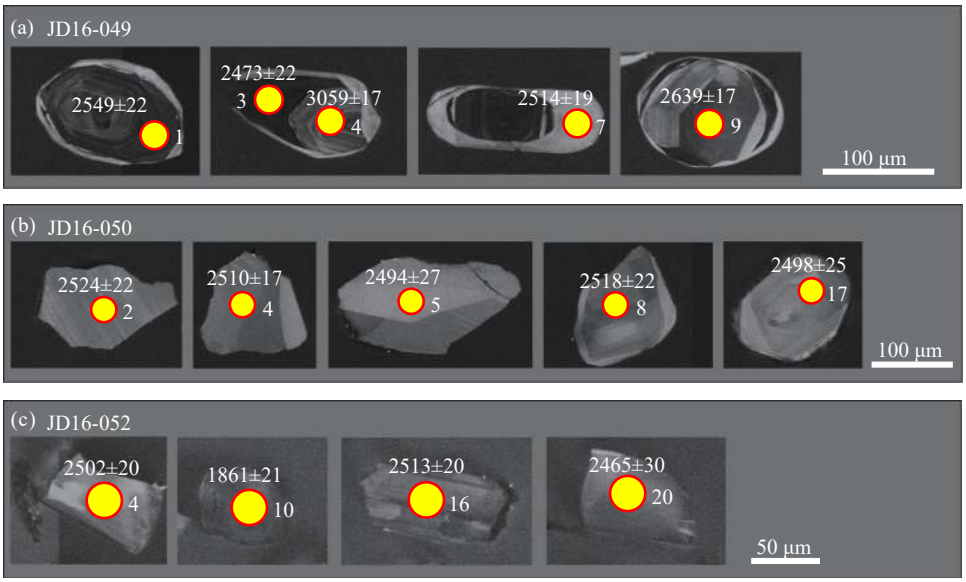

Fig. 3. CL images of representative zircon grains from samples JD16-049, JD16-050, and JD16-052 showing the inner structures and analysed locations.

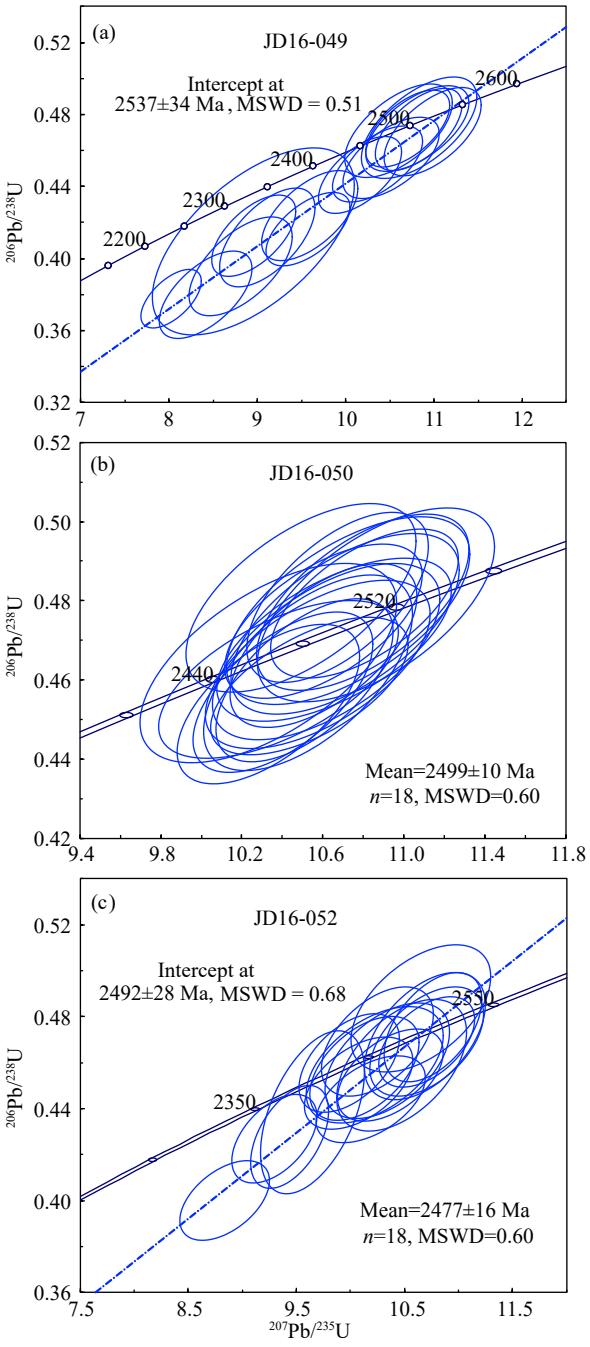

Fig. 4. Zircon U-Pb concordia diagram for granodioritic orthogneiss, syenogranite, and quartz syenite samples from the Malanyu Antiform. a –granodioritic orthogneiss; b –syenogranite (AG1); c–quartz syenite (AG2). The weighted mean age or upper intercept ages and MSWD are shown in each graph.

three structureless zircon rims (e.g. spot 7 in Fig. 3a). The zircons have Th/U values of 0.04 –2.99 and younger $^{207}Pb/^{206}Pb$ dates ranging from 2549 ± 22 Ma to 2394 ± 20 Ma. This large range of $^{207}Pb/^{206}Pb$ dates is interpreted as being due to radiogenic Pb-loss from a single-aged zircon population with an upper intercept date of 2537 ± 34 Ma (MSWD = 0.51) interpreted as the crystallisation age of the orthogneiss' protolith (Fig. 4a). Also, there are 12 analyses that plotted below the concordia curve, which are caused by later metamorphic or alteration events (Fig. 4a).

Zircons from the syenogranite sample (JD16-050, AG1) are 100 μm to 180 μm long, anhedral to subhedral in shape, with length/width ratios of 1∶1 to 2∶1. They have weak and blurry oscillatory growth zonation or are structureless (Fig. 3b), with Th/U ratios of 0.79 –1.50 (indicative of a magmatic origin). Eighteen analyses from the sample yield $^{207}Pb/^{206}Pb$ dates ranging from 2524 ± 22 Ma to 2468 ± 20 Ma with a weighted mean of 2499 ± 10 Ma (MSWD = 0.60; Fig. 4b; Appendix Table S1), which is interpreted as the crystallisation age of the syenogranite. Younger apparent $^{207}Pb/^{206}Pb$ dates of 2439 ± 21 Ma (spot 12) and 2331 ± 25 Ma (spot 10) are interpreted as recording younger metamorphic or alteration events in the region.

Twenty spots were analysed on 20 zircons from the quartz syenite sample (AG2, JD16-052). The zircons are subhedral to anhedral in shape, 50 –120 μm long, have length/width ratios of 1∶1 to 1.5∶1 and exhibit structureless inner textures on CL images (Fig. 3c). The zircons have a wide range of $^{207}Pb/^{206}Pb$ dates from 2522 ± 20 Ma to 1861 ± 21 Ma with Th/U ratios of 0.001–1.77. These dates can be divided into two groups, with the first consisting of 18 spots yielding $^{207}Pb/^{206}Pb$ dates of 2522 ± 20 Ma to 2431 ± 24 Ma with Th/U ratios of 0.02–1.77, and a weighted mean $^{207}Pb/^{206}Pb$ date of 2477 ± 16 Ma (MSWD = 2). Eleven of the 18 spots plot on the concordia curve whereas the other seven spots fall below the curve (Fig. 4c). Taken together, the 18 analyses yield an upper intercept date of 2492 ± 28 Ma (MSWD = 0.68), which is coeval with their weighted mean $^{207}Pb/^{206}Pb$ date of 2477 ± 16 Ma within error, and is interpreted as the crystallisation age of the quartz syenite. The second group consists of two analyses yielding a $^{207}Pb/^{206}Pb$ date of 2155 ± 34 Ma with a Th/U ratio of 0.001, and an 1836 ± 17 Ma date with a Th/U ratio of 0.002. These younger dates may represent the timing of metamorphic or alteration events in the region.

4.2. Major and trace elements

4.2.1. Major elements

The granodioritic orthogneiss, syenogranite, and quartz syenite were analysed for major and trace elements geochemistry (Appendix Table S2). The granodioritic orthogneiss sample is characterized by moderate SiO_2 (61.74%), Na_2O (3.54%) and K_2O (2.59%), and high MgO (4.10%), with an Mg# [100 × Mg/(Mg + Fe_{total})] of 51.86. In contrast, the granites have much higher SiO_2 (71.91% and 73.22%) and K_2O (7.52% and 8.37%) values, and much lower assays of the other major elements (Appendix Table S2). In addition, the A/CNK ratios [molar Al_2O_3/(CaO + Na_2O + K_2O)] of the granodioritic orthogneiss is 0.98 (metaluminous), syenogranite is 1.07 (weakly peraluminous), and quartz syenite is 1.05 (weakly peraluminous).

4.2.2. Trace elements

The granodioritic orthogneiss sample (JD16-049) has a total rare earth element (REE_T) content of 90.9×10^{-6} and exhibits a right-inclined pattern indicating the enrichment in

light rare earth elements (LREE) relative to heavy rare earth elements (HREE) with a $(La/Yb)_N$ ratio of 14.46, and positive Eu anomalies (Eu/Eu* = 1.35; Fig. 5a).

In contrast, the syenogranite and quartz syenite have lower total REE contents of 30.97×10^{-6} (AG1) and 25.93×10^{-6} (AG2), have more steeply right-inclined patterns, with higher $(La/Yb)_N$ ratios of 76.27 (AG1) and 146.24 (AG2), and pronounced positive Eu anomalies (Eu/Eu*) of 8.57 for AG1 and 27.04 for AG2 (Appendix Table S2; Fig. 5a).

On a primitive mantle-normalised trace element spider diagram (Fig. 5b), the granodioritic orthogneiss, syenogranite, and quartz syenite have similar trace element patterns, with depletion in Th, U, Nb, and Ti and enrichment in Rb, Ba, K, La, Ce, and P.

4.3. Sr and Nd isotopes

The Sr-Nd isotopic analytical results for the granodioritic orthogneiss, syenogranite, and quartz syenite are given in Appendix Table S2. The calculated initial $^{87}Sr/^{86}Sr$ ratio for the granodioritic orthogneiss is 0.70144, syenogranite (AG1) is 0.69194, and quartz syenite (AG2) is 0.70152 (further discussed below).

The granodioritic orthogneiss has an $\varepsilon Nd(t)$ value of 3.5 with a two-stage depleted mantle Nd model age (T_{2DM}) of 2619 Ma, whereas the syenogranite has an $\varepsilon Nd(t)$ value of 0.3 with a T_{2DM} age of 2841 Ma, and the quartz syenite has an $\varepsilon Nd(t)$ value of 1.3 with a T_{2DM} age of 2754 Ma.

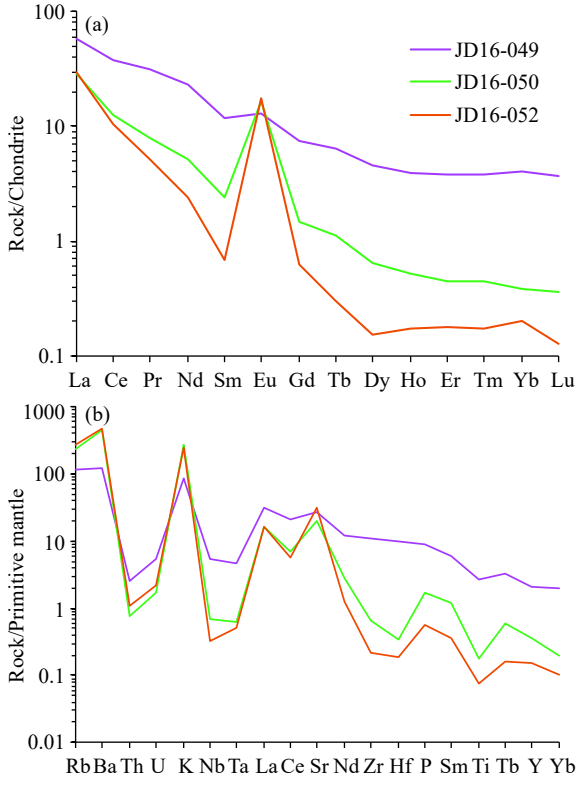

Fig. 5. Normalisation plots. a –chondrite-normalised REE plot; b–primitive mantle normalised element spider plot for the granodioritic orthogneiss, syenogranite, and quartz syenite in the Malanyu Antiform. Chondrite normalising values from Taylor SR and McLennan SM (1985), and primitive mantle normalised values from Sun SS and McDonough WF (1989).

4.4. Hf isotopes

The three samples dated above had *in-situ* zircon Hf isotopic measurements completed on their dated spots. The results are plotted in Fig. 6, and listed in Appendix Table S3.

Nine Lu-Hf isotopic analyses from the granodioritic orthogneiss (sample JD16-049) yielded $^{176}Hf/^{177}Hf$ ratios of 0.28115 to 0.281279, $\varepsilon Hf(t)$ values from −3.2 to +2.9 (for t = 2537 Ma), and t_{DM2} ages of 3253–2866 Ma (Appendix Table S3). Eighteen zircon grains from the syenogranite (AG1, sample JD16-050) have variable Hf isotopic compositions, with $^{176}Hf/^{177}Hf$ ratios between 0.28122 and 0.28131, $\varepsilon Hf(t)$ values between +0.57 and +3.82 (for t = 2499 Ma), and two-stage depleted mantle Hf model ages (t_{DM2}) between 2987 and 2779 Ma (Fig. 6; Appendix Table S3). Fourteen zircon grains from the quartz syenite (AG2; sample JD16-052) yielded $^{176}Hf/^{177}Hf$ ratios between 0.281126 and 0.28162, $\varepsilon Hf(t)$ values between +0.5 and +14.08 (for t = 2492 Ma), and t_{DM2} ages between 2986 Ma and 2112 Ma (Fig. 6; Appendix Table S3). Generally, the syenogranite and quartz syenite have much higher $\varepsilon Hf(t)$ values and younger two-stage depleted mantle Hf model ages than the granodioritic orthogneiss.

5. Discussion

5.1. Geochronology

The LA-ICP-MS zircon U-Pb zircon date of 2537 ± 34 Ma for the granodioritic orthogneiss is interpreted as the crystallisation age for its protolith, which is coeval with the dates of magmatic precursors for the dioritic and trondhjemitic orthogneisses dated between 2535 ± 23 Ma and 2513 ± 8 Ma in the region (Bai X et al., 2014). Two inherited

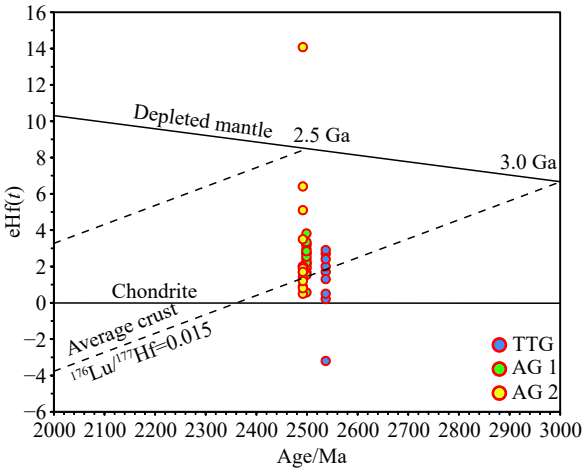

Fig. 6. Plot of zircon U-Pb ages *vs.* $\varepsilon Hf(t)$ values for zircons from the granodioritic orthogneiss, syenogranite, and quartz syenite in the Malanyu Antiform. The error bar for individual $\varepsilon Hf(t)$ value was not shown, as most of them have error range less than 1.0 unit, and thus within the symbol if plotted. All $\varepsilon Hf(t)$ values were calculated at the age of the rock.

zircon grains from the granodioritic orthogneiss have $^{207}Pb/^{206}Pb$ ages of 3059 ± 17 Ma and 2639 ± 17 Ma. The former date is identical within error with the $^{207}Pb/^{206}Pb$ zircon ages of tonalitic orthogneiss in the neighbouring Huangbaiyu area (Nutman AP et al., 2011), and the latter is coeval within error with metavolcanic rocks intruded by protoliths for the granodioritic orthogneiss in the region (Guo RR et al., 2013, 2015).

The 2499 ± 10 Ma (for AG1) and 2492 ± 28 Ma date for the syenogranite sample (AG2) are a little younger than a pegmatite with a U-Pb zircon age of 2503 ± 11 Ma that intrudes a fine-grained granulite-facies gneiss. The gneiss is located a few kilometres east of the study area and consists of K-feldspar, and minor amounts of quartz, white mica, garnet, and tourmaline. The age of the pegmatite is coeval with the granulite facies metamorphic age of 2503 ± 5 Ma (Nutman AP et al., 2011). These coincident ages show that the granulite-facies metamorphism is associated with anatexis and intrusion of coeval poorly foliated or non-foliated granitic dykes similar to the syenogranite and quartz syenite in the study area. It is proposed that the anatexis is related to decompression and remelting of the orthogneiss following the peak granulite facies metamorphism. One of the youngest $^{207}Pb/^{206}Pb$ age of 1836 ± 17 Ma for zircon from the quartz syenite is similar to the about 1850 Ma granulite in the Trans-North China Orogen (TNCO), which is interpreted as representing an uplifting and cooling age of granulite terranes following a crustal thickening event related to continental collision (Duan Z et al., 2015). The younger $^{207}Pb/^{206}Pb$ zircon date of 2155 ± 34 Ma from the quartz syenite possibly dates a thermal event, which is also indicated by similar zircon dates from orthogneiss in the region, the age of Paleoproterozoic metamafic dykes in Eastern Hebei and northern Liaoning provinces, and magmatic events in the Trans-North China Orogen and Jiao-Liao-Ji Belt (Guo RR et al., 2013; Wei CJ et al., 2014; Yuan LL et al., 2015; Duan Z et al., 2019). Therefore, as both the syenogranite (AG1) and quartz syenite (AG2) are neither foliated nor metamorphosed, the youngest age limit for the granulite-facies metamorphism in the region is constrained by the about 2500 Ma age of these granitic rocks. The implication is that the younger ages reported in the literature for the metamorphism are not the minimum age of the granitite-facies metamorphic event in the Eastern Zone of NCB.

5.2. Petrogenesis of the granodioritic orthogneiss, syenogranite, and quartz syenite

5.2.1. Petrogenesis of the granodioritic orthogneiss

Magmatic zircons analysed from granodioritic orthogneiss sample (JD16-049) have $\varepsilon Hf(t)$ values between −3.2 and +2.9, with most lying between the evolutionary lines for chondrite and the depleted mantle (Fig. 6). This indicates that the granodioritic magma was derived from partial melting of a depleted mantle, or partial melting of juvenile basaltic precursors derived from a depleted mantle, with a minor contribution from the crust. This is supported by the xenocrystic zircons in the granodioritic orthogneiss. The $\varepsilon Hf(t)$ values obtained in this study are similar to those from metadioritic and trondhjemitic orthogneiss in the region with values of +1.5 to +5.3 (Bai X et al., 2014). This indicates that the magmatic precursors of the gneisses have similar petrogenetic histories and tectonic settings.

Geochemical data reveal that the granodioritic orthogneiss sample displays a high MgO content of 4.1% with a Mg# of 51.86. Previous experimental studies have found that partial melting of a single basalt composition can provide a Mg# value no greater than about 48 (Rapp RP et al., 1999). Combined with the $\varepsilon Hf(t)$ values, it is suggested that the magmatic precursor for the granodioritic orthogneiss is similar to those of the metadioritic and trondhjemitic orthogneisses, which are derived from a depleted mantle (Bai X et al., 2014; Rapp RP and Watson EB, 1995; Yang JH et al., 2008). Bai X et al. (2014) propose that the Neoarchean dioritic magma was derived from a mantle source that had been modified by reaction with felsic slab-derived melts. Although the granodioritic orthogneiss plots in the high-silica adakite (HSA) field in Fig. 7, its major geochemical characteristics and crystallisation age are similar to the metadioritic and trondhjemitic orthogneisses. The granodioritic orthogneiss, therefore, is derived from fractional crystallisation of a dioritic magma, instead of partial melting of a subducted slab (Bai et al., 2014).

5.2.2. Petrogenesis of the anatectic granites

Anatectic or partial melts form in the lower part of the crust or mantle where temperatures are higher than the solidus producing migmatites (Zheng YF and Hermann J, 2014). Furthermore, anatectic melts are derived from incongruent melting of source rocks with the least differentiation. The syenogranite and quartz syenite in this study exhibit transitional (or gradational) relationships with the granodioritic orthogneiss, indicating a genetic relationship.

Compared to the granodioritic orthogneiss, the syenogranite and quartz syenite are enriched in SiO_2, K_2O, Eu, Rb, Ba, and depleted in all other major and trace elements, which are likely concentrated in mafic residues. The Sr only has small variations between these two rocks. These characteristics show that Si, and large ion lithophile elements (LILE), such as K, Rb, and Ba, readily enter the melts during anatexis. The LREE and HREE from the syenogranite and quartz syenite generally experienced strong magmatic differentiation with $(La/Yb)_N$ ratios of 76.27 (AG1) and 146.24 (AG2) (Fig. 5), except for Eu^{2+} that is easily accommodated at the alkali-site in the K-feldspar and typically induces a positive anomaly (Larsen RB, 2002). Therefore, the syenogranite and quartz syenite are the products of partial melting of the source rocks similar in composition with the granodioritic orthogneiss.

All zircons from the granodioritic orthogneiss, syenogranite, and quartz syenite exhibit steep HREE patterns with a positive Ce, with most having negative Eu anomalies (Appendix Table S4; Fig. 8). However, the U and Th contents of zircons from the granodioritic orthogneiss, syenogranite, and quartz syenite are different (Appendix Table S1; Fig. 9). Among these three rock types, the quartz syenite has the highest U concentration ranging from 673×10^{-6} to 4225×10^{-6}

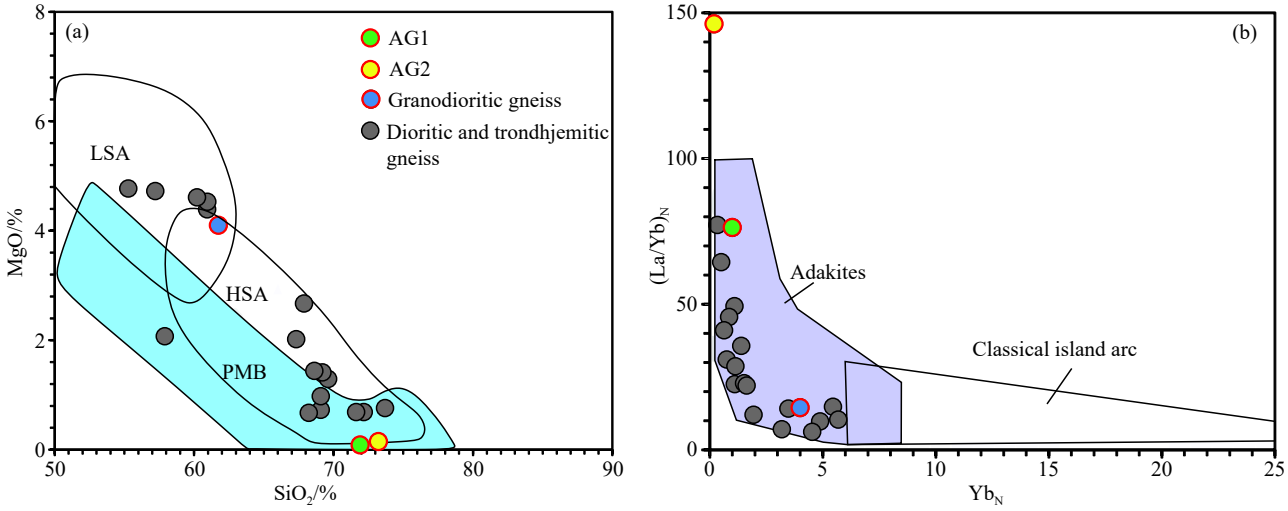

Fig. 7. Petrogenetic discrimination diagrams for granodioritic orthogneiss. a–MgO vs SiO_2 plot (after Martin H et al., 2005); b–$(La/Yb)_N$ vs Yb_N plot discriminating between adakitic and classical arc calc-alkaline compositions (after Martin H, 1986). The data of dioritic and trondhjemitic gneisses were cited from Bai X et al. (2014). PMB–experimental partial melts from basalts or amphibolites; LSA–low-silica adakite; HSA–high-silica adakite.

and the widest Th variation between 3×10^{-6} and 1683×10^{-6}. In contrast, the syenogranite has the lowest U concentration ranging from 14×10^{-6} to 48×10^{-6} and the narrowest Th range between 14×10^{-6} and 68×10^{-6}. Similarly, the REE concentrations of zircons from the quartz syenite are the highest among these three rock types. These differences in U, Th, and REE in the zircons may be caused by the distinctive T and P during the anatexis forming the syenogranite and quartz syenite, which is analogues to the zircons in the Ivrea Zone of Italy (Vavra G et al., 1999). Zircon overgrowths formed during upper amphibolite facies at the low growth rate in the Ivrea Zone have U contents between 1008 μg/g and 2279 μg/g, which is higher than those formed during granulite facies at high growth rates, with zircon U contents ranging from 53 μg/g to 127 μg/g (Vavra G et al., 1999). The obvious implication is that the granodioritic orthogneiss was formed earlier at a higher-pressure during granulite-facies than the quartz syenite.

The granodioritic orthogneiss and quartz syenite have similar initial $^{87}Sr/^{86}Sr$ ratios, but the syenogranite has an abnormal initial $^{87}Sr/^{86}Sr$ ratio due to its high $^{87}Rb/^{86}Sr$ value. This could have resulted from a rapid partial melting causing the disequilibrium of the Rb-Sr isotope system, as Sr tends to be enriched in early crystallised calcium plagioclase leaving Rb in the liquid phase to eventually enter potassium-bearing minerals. Although it is reasonable to suggest that the $\varepsilon Nd(t)$ values of the syenogranite and quartz syenite, being the products of partial melting, are lower than that of the granodioritic orthogneiss, the difference between them shows that the syenogranite and quartz syenite did not fully inherit the Sr-Nd isotope system of the granodioritic orthogneiss. In other words, the Sr-Nd isotopes of the syenogranite and quartz syenite cannot reflect their source rock (i.e. granodioritic orthogneiss). In addition, the syenogranite and quartz syenite, and granodioritic orthogneiss have different $\varepsilon Hf(t)$ values, which will be discussed below.

Biotite starts to breakdown around 850℃ at 1000 MPa (Vielzeuf D and Holloway JR, 1988). These are similar conditions to the estimated peak P-T values of 900–1030 MPa at 860–950℃ in Eastern Hebei Province (Duan Z et al., 2017; Kwan LCJ et al., 2016). Biotite can therefore breakdown at these conditions during granulite metamorphism leading to partial-melting of the granodioritic orthogneiss, and the formation of the syenogranite and quartz syenite.

5.2.3. Hf isotope data discrepancy

Zircons contain the highest levels and least radiogenic Hf isotope compositions in crustal rocks. This means that zircons crystallising from partial melts usually show similar $^{176}Hf/^{177}Hf$ ratios as relict zircons whose dissolution dominates the budget of Hf in melts. It is noted that the granodioritic orthogneiss and syenogranite from the Malanyu Antiform have a similar narrow range of $\varepsilon Hf(t)$ values measured in this study. Zircons from the quartz syenite, however, have a much wider range and elevated $\varepsilon Hf(t)$ values of +0.5 to +14.08 compared to the range of −3.2 to +2.9 for the granodioritic orthogneiss. The implication is that the Hf isotope composition of zircons crystallising from partial melts and accompanying magmatic zircons do not necessarily reflect the Hf isotope composition of their source rocks. Examples are found in leucosomes and associated granitic rocks in the Weihai UHP Terrane of the Sulu Orogeny in east-central China, where $\varepsilon Hf(t)$ values for magmatic and anatexis-related zircons are elevated by 10 units, which is analogous to the zircons in the syenogranite and quartz syenite in our study (Liu FL et al., 2009, 2010). Other examples are found at the Mayuan Metamorphic Complex of the Cathaysian Terrane in southeastern China (Liu R et al., 2010), granites from the Peninsula Pluton in South Africa (Farina F et al., 2014), migmatite from the Higo Metamorphic Terrane in Japan (Maki K et al., 2014), Antarctic Peninsula (Flowerdew MJ et al., 2006), and Kinawa in the São Francisco Craton of Brazil (Carvalho BB et al., 2017). In these examples, the elevated $\varepsilon Hf(t)$ values could be attributed to the anatectic effects on the

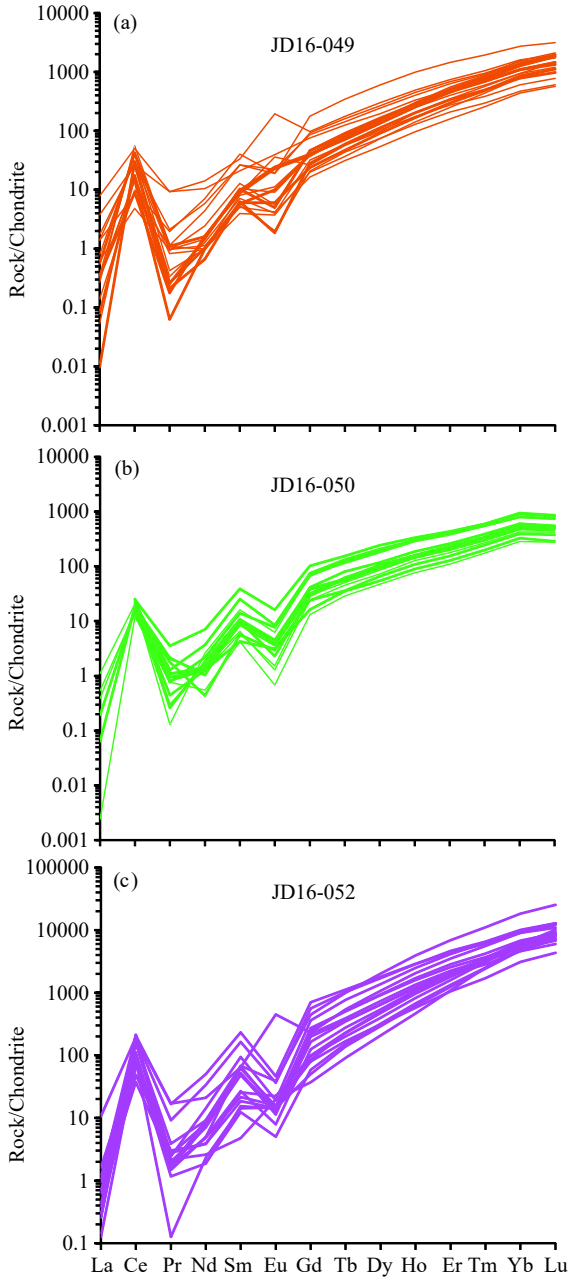

Fig. 8. Chondrite-normalised REE patterns of analysed zircons from samples. a –JD16-049; b –JD16-050; c –JD16-052. Chondrite normalising values from Taylor SR and McLennan SM (1985).

zircon Lu-Hf isotopic system, where the Hf is not bound in zircons and constitutes an important proportion of Hf in the anatectic melts (Liu FL et al., 2010; Farina F et al., 2014; Chen YX et al., 2015).

In principle, Hf in an anatectic melt may be derived from two components in a closed system. The first is from the dissolution of zircons in the source rock (zircon-Hf), and the second is from the other Hf-bearing minerals during anatexis in the crust (Chen YX et al., 2015). The relative contribution of these two Hf types depends on the melt reaction and dynamics (i.e. the rates of partial melting and melt extraction), which can greatly influence the dissolution kinetics of zircons in partial melts (Tang M et al., 2014).

Zircon is the dominant Hf carrier in most granitic rocks,

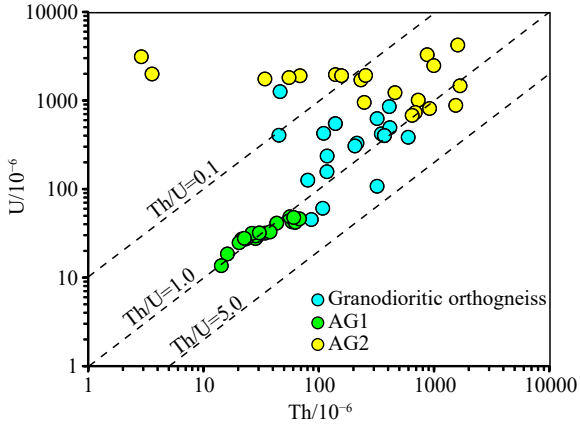

Fig. 9. Th vs U diagram for the zircons from the granodioritic orthogneiss, syenogranite, and quartz syenite in the Malanyu Antiform.

whereas the Hf contents of common rock-forming minerals are very low, typically $<10\times10^{-6}$, except titanite that may have higher contents reaching about 130×10^{-6} (Bea F et al., 2006). The amphibole in calc-alkaline tonalite to monzogranite can contain around 2×10^{-6} Hf, and orthopyroxene in felsic granulite can contain around 1×10^{-6} Hf (Bea F et al., 2006). Although these common rock-forming minerals have much lower Hf contents than zircon, they can also be important sources for Hf due to their high modal abundances in crustal rocks (Chen YX et al., 2015).

The granodioritic orthogneiss in the study area contains a large proportion of the mafic minerals orthopyroxene, amphibole, and biotite, which are potential sources for Hf in addition to zircon. Therefore, the break-down of these Hf-bearing major minerals in anatectic reactions causes the dissolution of Hf into partial melts, resulting in elevated $^{176}Hf/^{177}Hf$ ratios for zircons crystallised from such melts. Consequently, it does not need an external source with high $^{176}Hf/^{177}Hf$ ratios (Maki K et al., 2014). Thus, the elevated $\varepsilon Hf(t)$ values in the quartz syenite sample (AG2) are interpreted to be sourced from Hf-bearing minerals such as orthopyroxene, amphibole, and biotite during partial melting of the granodioritic orthogneiss. Although the rapid extraction and ascent of partial melts can preserve the original isotopic heterogeneity of the source rocks, sufficient merging of melts can obscure such heterogeneity (Chen YX et al., 2017). Such a scenario is regarded as being unlikely given that the transitional relationship between the granodioritic orthogneiss, syenogranite, and quartz syenite.

5.3. Implication to the geological evolution in Eastern Hebei Province

Although a Neoarchean mantle plume has been proposed as the geodynamic setting in the Eastern Hebei Province (Zhao GC et al., 1998, 1999; Geng YS et al., 2006, 2016; Yang JH et al., 2008), a subduction-related setting at a convergent plate margin is also proposed in the literature (Nutman AP et al., 2011; Zhang LC et al., 2012; Guo RR et al., 2013, 2014, 2015; Bai X et al., 2014, 2015, 2016). Bai X et al. (2014, 2015) propose that the subduction-related granites and charnockites in the region have crystallisation

ages of 2535–2513 Ma, and Guo RR et al. (2013, 2015) suggest that arc-related metavolcanic rocks have a magmatic crystallisation age spanning 2614–2511 Ma. If the 2545–2523 Ma BIF and 2527–2511 Ma magmatic protoliths of the monzogranitic and syenogranitic orthogneisses formed in a back-arc basin (Fu J et al., 2017; Li LX et al., 2015), the youngest limit of subduction is confined at 2511 Ma. The subsequent upper amphibolite- to granulite-facies metamorphism recorded by the Archean metavolcanic units and orthogneiss in Eastern Hebei Province would have taken place between 2511 Ma and 2500 Ma (Yang JH et al., 2008; Nutman AP et al., 2011; Wang W et al., 2013, 2015; Fu J et al., 2017; Yang C and Wei C, 2017). Such deep-seated metamorphism would be related to the collision of continental terranes during crustal thickening and subsequent emplacement of the 2499 Ma syenogranite and 2492 Ma quartz syenite. This places the period between collisional, granulite-facies metamorphism, and anatexis at around 10×10^6 years. Such a limited time span and intense tectonic-metamorphism coincide with the tectonic-thermal event recording the Neoarchean amalgamation of multiple terranes throughout NCB during about 2500 Ma (Zhai MG and Santosh M, 2011; Wan YS et al., 2015; Peng P, 2016; Zhai M and Zhu X, 2016; Shi Y and Zhao X, 2017). Furthermore, the deformation appears to be stronger than many Archean cratons characterised by about 2700 Ma tectonic events (Condie KC et al., 2009), but appears to be similar to the latest Archean magmatism and orogenesis present in the Dharwar Craton of India, the Napier Complex and Vestfold Hills of Antarctica, North Australian Craton, and Gawler Craton in southern Australia (Zhao G et al., 2003; Swain G et al., 2005; Zulbati F and Harley SL, 2007; Cawood PA and Korsch RJ, 2008; Nelson DR, 2008). The regional granulite grade metamorphism and crustal thickening took place in the Gawler Craton during the 2500–2400 Ma Sleafordian Orogeny, which was driven by the collision between continental components, leading to the formation of a continental interior (Swain G et al., 2005). This was coeval with the emplacement of the protoliths for the 2510 Ma orthogneiss in the North Australia Craton (Pirajno F and Bagas L, 2008). Granulites facies metamorphic events dared at about 2500 Ma are also documented in the Dharwar Craton of India and Vestfold Hills of Antarctica (Zhao G et al., 2003; Zulbati F and Harley SL, 2007). The synchronosity of this apparently widespread metamorphic and tectonic event could be due to these cratons being linked during the late Neoarchean.

6. Conclusion

The LA-ICP-MS zircon U-Pb dating shows that syenogranite and quartz syenite sourced from partial melts of a granodioritic orthogneiss were emplaced during about 2500 Ma at the end of granulite-facies metamorphism. Based on the geological and geochemical studies, the about 2500 Ma non-foliated granites are interpreted to be the product of rapid partial-melting of the granodioritic orthogneiss spanning a period of around 10×10^6 years between 2511 Ma and 2499 Ma. Furthermore, the Sr-Nd-Hf isotopic geochemistry of the granodioritic orthogneiss, syenogranite, and quartz syenite shows that there was an isotope disequilibrium between the orthogneiss and granites. The 2511 Ma to 2499 Ma tectonic-metamorphism in NCB is similar to those in the Dharwar Craton of India, the Napier Complex, and Vestfold Hills of Antarctica, North Australian Craton, and Gawler Craton in southern Australia, indicating a spatial connection between these regions during the Neoarchean.

CRediT authorship contribution statement

Si-Hong Jiang conceived of the presented idea. Si-Hong Jiang developed the theory and performed the computations. Leon Bagas improved the theory. All authors discussed the results and contributed to the final manuscript.

Declaration of competing interest

The authors declare no conflicts of interest.

Acknowledgment

The authors wish to thank Ms. Mu Liu for her assistance in the whole-rock geochemical and Sr-Nd isotope analyses at the Analytical Center at the Beijing Institute of Geology for Nuclear Industry (ACBIGNI). The authors also thank Ms. Hai-feng Hou and Mr. Zheng-huan Zhao for LA-ICP-MS U-Pb zircon and Lu-Hf isotope analyses at the Beijing Createch Testing Technology Co. Ltd. The CAGS Research Fund (YYWF201715, YK1608), and the project of China Geological Survey (DD20190437) financially support this study and contribution. Thoughtful comments by two anonymous reviewers have considerably improved the manuscript.

Appendix data

Supplementary data (Appendix Table S1–S4) to this article can be found online at doi: 10.31035/cg2021014.

References

Aranovich LY, Makhluf AR, Manning CE, Newton RC. 2014. Dehydration melting and the relationship between granites and granulites. Precambrian Research, 253, 26–37. doi: 10.1016/j.precamres.2014.07.004.

Ayres M, Harris N. 1997. REE fractionation and Nd-isotope disequilibrium during crustal anatexis: Constraints from Himalayan leucogranites. Chemical Geology, 139, 249–269. doi: 10.1016/S0009-2541(97)00038-7.

Bai X, Liu SW, Guo RR, Wang W. 2015. Zircon U-Pb-Hf isotopes and geochemistry of two contrasting Neoarchean charnockitic rock series in Eastern Hebei, North China Craton: Implications for petrogenesis and tectonic setting. Precambrian Research, 267, 72–93. doi: 10.1016/j.precamres.2015.06.004.

Bai X, Liu SW, Guo RR, Wang W. 2016. A Neoarchean arc–back-arc system in Eastern Hebei, North China Craton: Constraints from zircon U-Pb-Hf isotopes and geochemistry of dioritic-tonalitic-trondhjemitic-granodioritic (DTTG) gneisses and felsic paragneisses. Precambrian Research, 273, 90–111. doi: 10.1016/j.precamres.2015.12.003.

Bai X, Liu SW, Guo RR, Zhang LF, Wang W. 2014. Zircon U-Pb-Hf isotopes and geochemistry of Neoarchean dioritic-trondhjemitic

gneisses, Eastern Hebei, North China Craton: Constraints on petrogenesis and tectonic implications. Precambrian Research, 251, 1–20. doi: 10.1016/j.precamres.2014.05.027.

Barker F. 1979. Trondhjemite: Definition, environment and hypotheses of origin: Trondhjemites, dacites and related rocks. Amsterdam, Elsevier, 1–12.

Bea F, Montero P, Ortega M. 2006. A LA-ICP-MS evaluation of Zr reservoirs in common crustal rocks: Implications for Zr and Hf geochemistry, and zircon-forming processes. Canadian Mineralogist, 44, 693–714. doi: 10.2113/gscanmin.44.3.693.

Blichert-Toft J, Albarède F. 1997. The Lu-Hf isotope geochemistry of chondrites and the evolution of the mantle-crust system. Earth and Planetary Science Letters, 148, 243–258. doi: 10.1016/S0012-821X(97)00040-X.

Burnham CW. 1967. Hydrothermal fluids at the magmatic stage. In: Barnes HL (eds.), Geochemistry of hydrothermal ore deposits. New York, Holt, Reinhart and Winston, 38–76.

Carvalho BB, Janasi VA, Sawyer EW. 2017. Evidence for Paleoproterozoic anatexis and crustal reworking of Archean crust in the São Francisco Craton, Brazil: A dating and isotopic study of the Kinawa migmatite. Precambrian Research, 291, 98–118. doi: 10.1016/j.precamres.2017.01.019.

Cawood PA, Korsch RJ. 2008. Assembling Australia: Proterozoic building of a continent. Precambrian Research, 166, 1–38. doi: 10.1016/j.precamres.2008.08.006.

Chen MY, Li SX. 1996. The evolution of granulite facies metamorphism in eastern Hebei province. Acta Petrologica Sinica, 12(2), 343–357 (in Chinese with English abstract).

Chen YX, Gao P, Zheng YF. 2015. The anatectic effect on the zircon Hf isotope composition of migmatites and associated granites. Lithos, 238, 174–184. doi: 10.1016/j.lithos.2015.09.026.

Chen YX, Zhou K, Gao XY. 2017. Partial melting of ultrahigh-pressure metamorphic rocks during continental collision: Evidence, time, mechanism, and effect. Journal of Asian Earth Sciences, 145, 177–191. doi: 10.1016/j.jseaes.2017.03.020.

Chu NC, Taylor RN, Chavagnac V, Nesbitt RW, Boella RM, Milton JA, German CR, Bayon G, Burton K. 2002. Hf isotope ratio analysis using multi-collector inductively coupled plasma mass spectrometry: An evaluation of isobaric interference corrections. Journal of Analytical Atomic Spectrometry, 17, 1567–1574. doi: 10.1039/b206707b.

Clemens JD, Droop GTR. 1998. Fluids, P-T paths and the fates of anatectic melts in the Earth's crust. Lithos, 44, 21–36. doi: 10.1016/S0024-4937(98)00020-6.

Clemens JD, Vielzeuf D. 1987. Constraints on melting and magma production in the crust. Earth and Planetary Science Letters, 86, 287–306. doi: 10.1016/0012-821X(87)90227-5.

Clemens JD. 1984. Water contents of silicic to intermediate magmas. Lithos, 17, 273–287. doi: 10.1016/0024-4937(84)90025-2.

Condie KC, Belousova E, Griffin WL, Sircombe KN. 2009. Granitoid events in space and time: Constraints from igneous and detrital zircon age spectra. Gondwana Research, 15, 228–242. doi: 10.1016/j.gr.2008.06.001.

Davies GR, Tommasini S. 2000. Isotopic disequilibrium during rapid crustal anatexis: Implications for petrogenetic studies of magmatic processes. Chemical Geology, 162, 169–191. doi: 10.1016/S0009-2541(99)00123-0.

Dong C, Xie H, Kröner A, Wan S, Liu S, Xie S, Song Z, Ma M, Liu D, Wan Y. 2017. The complexities of zircon crystallization and overprinting during metamorphism and anatexis: An example from the late Archean TTG terrane of western Shandong Province, China. Precambrian Research, 300, 181–200. doi: 10.1016/j.precamres.2017.07.034.

Duan Z, Wei C, Li Z. 2019. Metamorphic P-T paths and zircon U-Pb ages of Paleoproterozoic metabasic dykes in eastern Hebei and northern Liaoning: Implications for the tectonic evolution of the North China Craton. Precambrian Research, 326, 124–141. doi: 10.1016/j.precamres.2017.11.001.

Duan Z, Wei C, Qian J. 2015. Metamorphic P-T paths and Zircon U-Pb age data for the Paleoproterozoic metabasic dykes of high-pressure granulite facies from Eastern Hebei, North China Craton. Precambrian Research, 271, 295–310. doi: 10.1016/j.precamres.2015.10.015.

Duan Z, Wei C, Rehman HU. 2017. Metamorphic evolution and zircon ages of pelitic granulites in eastern Hebei, North China Craton: Insights into the regional Archean P-T-t history. Precambrian Research, 292, 240–257. doi: 10.1016/j.precamres.2017.02.008.

Farina F, Stevens G, Gerdes A, Frei D. 2014. Small-scale Hf isotopic variability in the Peninsula pluton (South Africa): The processes that control inheritance of source $^{176}Hf/^{177}Hf$ diversity in S-type granites. Contributions to Mineralogy and Petrology, 168, 1–18. doi: 10.1007/s00410-014-1065-8.

Flowerdew MJ, Millar IL, Vaughan APM, Horstwood MSA, Fanning CM. 2006. The source of granitic gneisses and migmatites in the Antarctic Peninsula: A combined U-Pb SHRIMP and laser ablation Hf isotope study of complex zircons. Contributions to Mineralogy and Petrology, 151, 751–768. doi: 10.1007/s00410-006-0091-6.

Fu J, Liu S, Wang M, Chen X, Guo B, Hu F. 2017. Late Neoarchean monzogranitic-syenogranitic gneisses in the Eastern Hebei-Western Liaoning Province, North China Craton: Petrogenesis and implications for tectonic setting. Precambrian Research, 303, 392–413. doi: 10.1016/j.precamres.2017.05.002.

Gardiner NJ, Johnson TE, Kirkland CL, Smithies RH. 2017. Melting controls on the lutetium-hafnium evolution of Archaean crust. Precambrian Research, 305, 479–488. doi: 10.1016/j.precamres.2017.12.026.

Geng YS, Liu FL, Yang CH. 2006. Magmatic event at the end of the Archean in Eastern Hebei Province and its geological implication. Acta Geologica Sinica (English Edition), 80, 819–833. doi: 10.1111/j.1755-6724.2006.tb00305.x.

Geng YS, Shen QH, Du LL, Song HX. 2016. Regional metamorphism and continental growth and assembly in China. Acta Petrologica Sinica, 32(9), 2579–2608 (in Chinese with English abstract).

Geng YS, Shen QH, Song HX. 2018. Metamorphic petrology and geology in China: A review. China Geology, 1, 137–157. doi: 10.31035/cg2018012.

Geological Survey of Hebei Province. 1970. Geological Map of Qinglong Sheet at a scale of 1∶200000. Internal report, 1–40 (in Chinese).

Grant JA. 1985. Phase equilibria in partial melting of pelitic rocks. In: Ashworth JR (eds.), Migmatites. Glascow, Blackie and Son, 86–144.

Griffin WL, Wang X, Jackson SE, Pearson NJ, O'Reilly SY, Xu X, Zhou X. 2002. Zircon chemistry and magma mixing, SE China: *In-situ* analysis of Hf isotopes, Tonglu and Pingtan igneous complexes. Lithos, 61, 237–269. doi: 10.1016/S0024-4937(02)00082-8.

Guo RR, Liu SW, Bai X, Zhang LF, Wang W, Hu FY, Yan M. 2014. Geochemistry and zircon U-Pb chronology of Shuangshanzi Group in the eastern Hebei province, North China Craton: Constraints on petrogenesis and tectonic setting. Acta Petrologica Sinica, 30(10), 2885–2904 (in Chinese with English abstract).

Guo RR, Liu SW, Santosh M, Li QG, Bai X, Wang W. 2013. Geochemistry, zircon U-Pb geochronology and Lu-Hf isotopes of metavolcanics from eastern Hebei reveal Neoarchean subduction tectonics in the North China Craton. Gondwana Research, 24, 664–686. doi: 10.1016/j.gr.2012.12.025.

Guo RR, Liu SW, Wyman D, Bai X, Wang W, Yan M, Li QG. 2015. Neoarchean subduction: A case study of arc volcanic rocks in Qinglong-Zhuzhangzi area of the Eastern Hebei Province, North China Craton. Precambrian Research, 264, 36–62. doi: 10.1016/j.precamres.2015.04.007.

He GP, Ye HW. 1992. The evolution of metamorphism in granulite facies terrane, Eastern Hebei Province. Acta Petrologica Sinica, 8(2), 129–135 (in Chinese with English abstract).

Hou KJ, Li YH, Tian YY. 2009. *In situ* U-Pb zircon dating using laser ablation-multi ion counting-ICP-MS. Mineral Deposits, 28(4), 481–492 (in Chinese with English abstract).

Hou KJ, Li YH, Zou TR, Qu XM, Shi YR, Xie GQ. 2007. Laser ablation-MC-ICP-MS technique for Hf isotope microanalysis of zircon and its geological applications. Acta Petrologica Sinica, 23(10), 2595–2604 (in Chinese with English abstract).

Huang H, Niu Y, Mo X. 2017. Garnet effect on Nd-Hf isotope decoupling: Evidence from the Jinfosi batholith, Northern Tibetan Plateau. Lithos, 274–275, 31–38. doi: 10.1016/j.lithos.2016.12.025.

Jackson SE, Pearson NJ, Griffin WL, Belousova EA. 2004. The application of laser ablation-inductively coupled plasma-mass spectrometry (LA-ICP-MS) to in situ U-Pb zircon geochronology. Chemical Geology, 211, 47–69. doi: 10.1016/j.chemgeo.2004.06.017.

Jiang SH, Bagas L, Liu YF, Zhang LL. 2018. Geochronology and petrogenesis of the granites in Malanyu Anticline in eastern North China Block. Lithos, 312 –313, 21–37. doi: 10.1016/j.lithos.2018.04.028.

Kriegsman LM. 2001. Partial melting, partial melt extraction and partial back reaction in anatectic migmatites. Lithos, 56, 75–96. doi: 10.1016/s0024-4937(00)00060-8.

Kwan LCJ, Zhao GC, Yin CQ, Geng HY. 2016. Metamorphic P-T path of mafic granulites from Eastern Hebei: Implications for the Neoarchean tectonics of the Eastern Block, North China Craton. Gondwana Research, 37, 20–38. doi: 10.1016/j.gr.2016.05.004.

Larsen RB. 2002. The distribution of rare-earth elements in K-feldspar as an indicator of the petrogenetic processes in granitic pegmatites: Examples from two pegmatite fields in Southern Norway. Canadian Mineralogist, 40, 137–151. doi: 10.2113/gscanmin.40.1.137.

Li LX, Li HM, Xu YX, Chen J, Yao T, Zhang LF, Yang XQ, Liu MJ. 2015. Zircon growth and ages of migmatites in the Algoma-type BIF-hosted iron deposits in Qianxi Group from eastern Hebei Province, China: Timing of BIF deposition and anatexis. Journal of Asian Earth Sciences, 113, 1017–1034. doi: 10.1016/j.jseaes.2015.02.007.

Lin Q, Wu FY, Liu SW, Ge WC, Sun JG, Yin JZ. 1992. Archean Granites in the East of North China Platform. Beijing, Science Press, 1–220 (in Chinese).

Liou P, Guo J, Huang G, Fan W. 2019. 29 Ga magmatism in Eastern Hebei, North China Craton. Precambrian Research, 326, 6–23. doi: 10.1016/j.precamres.2017.11.002.

Liu DY, Nutman AP, Compston W, Wu JS, Shen QH. 1992. Remnants of ⩾3800 Ma crust in the Chinese part of the Sino-Korean craton. Geology, 20, 339–342. doi: 10.1130/0091-7613(1992)020<0339:ROMCIT>2.3.CO;2.

Liu F, Liu L, Cai J, Liu P, Wang F, Liu C, Liu J. 2019. A widespread Paleoproterozoic partial melting event within the Jiao-Liao-Ji Belt, North China Craton: Zircon U-Pb dating of granitic leucosomes within pelitic granulites and its tectonic implications. Precambrian Research, 326, 155–173. doi: 10.1016/j.precamres.2017.10.017.

Liu FL, Robinson PT, Gerdes A, Xue HM, Liu PH, Liou JG. 2010a. Zircon U-Pb ages, REE concentrations and Hf isotope compositions of granitic leucosome and pegmatite from the north Sulu UHP terrane in China: Constraints on the timing and nature of partial melting. Lithos, 117, 247–268. doi: 10.1016/j.lithos.2010.03.002.

Liu FL, Xue HM, Liu PH. 2009. Partial melting time of ultrahigh-pressure metamorphic rocks in the Sulu UHP terrane: Constrained by zircon U-Pb ages, trace elements and Lu-Hf isotope compositions of biotite-bearing granite. Acta Petrologica Sinica, 25(5), 1039–1055 (in Chinese with English abstract).

Liu R, Zhou H, Zhang L, Zhong Z, Zeng W, Xiang H, Jin S, Lu X, Li C. 2010. Zircon U-Pb ages and Hf isotope compositions of the Mayuan migmatite complex, NW Fujian Province, Southeast China: Constraints on the timing and nature of a regional tectonothermal event associated with the Caledonian orogeny. Lithos, 119, 163–180. doi: 10.1016/j.lithos.2010.06.004.

Liu SJ, Wan YS, Sun HY, Nutman AP, Xie HQ, Dong CY, Ma MZ, Liu DY, Jahn BM. 2013. Paleo- to Eoarchean crustal evolution in eastern Hebei, North China Craton: New evidence from SHRIMP U-Pb dating and in-situ Hf isotopic study of detrital zircons from paragneisses. Journal of Asian Earth Sciences, 78, 4–17. doi: 10.1016/jjseaes.2013.07.041.

Liu YS, Gao S, Hu ZC, Gao CG, Zong KQ, Wang DB. 2010c. Continental and oceanic crust recycling-induced melt-peridotite interactions in the Trans-North China Orogen: U-Pb dating, Hf isotopes and trace elements in zircons from mantle xenoliths. Journal of Petrology, 51, 537–571. doi: 10.1093/petrology/egp082.

Liu ZH, Yang ZS. 1994. The tectonic evolution of Archean high-grade metamorphic terrane, eastern Hebei, China. Journal of Changchun University of Earth Sciences, 24(3), 254–258 (in Chinese with English abstract).

London D, Morgan VI GB, Acosta-Vigil A. 2012. Experimental simulations of anatexis and assimilation involving metapelite and granitic melt. Lithos, 153, 292–307. doi: 10.1016/j.lithos.2012.04.006.

Ludwig KR. 2003. ISOPLOT 3.00: A Geochronological Toolkit for Microsoft Excel, Berkeley Geochronology Center. Special Publication 4.

Maki K, Yui TF, Miyazaki K, Fukuyama M, Wang KL, Martens U, Grove M, Liou JG. 2014. Petrogenesis of metatexite and diatexite migmatites determined using zircon U-Pb age, trace element and Hf isotope data, Higo metamorphic terrane, central Kyushu, Japan. Journal of Metamorphic Geology, 32, 301–323. doi: 10.1111/jmg.12073.

Martin H, Smithies RH, Rapp R, Moyen JF, Champion D. 2005. An overview of adakite, tonalite-trondhjemite-granodiorite (TTG), and sanukitoid: Relationships and some implications for crustal evolution. Lithos, 79, 1–24. doi: 10.1016/j.lithos.2004.04.048.

Martin H. 1986. Effect of steeper Archean geothermal gradient on geochemistry of subduction-zone magmas. Geology, 14, 753–756. doi: 10.1130/0091-7613(1986)14<753:EOSAGG>2.0.CO;2.

Morel MLA, Nebel O, Nebel-Jacobsen YJ, Vroon PZ. 2008. Hafnium isotope characterization of the GJ-1 zircon reference material by solution and laser-ablation MC-ICPMS. Chemical Geology, 255, 231–235. doi: 10.1016/j.chemgeo.2008.06.040.

Nelson DR. 2008. Geochronology of the Archean of Australia. Australian Journal of Earth Sciences, 55(6–7), 779–793. doi: 10.1080/08120090802094135.

Newton RC, Touret JLR, Aranovich LY. 2014. Fluids and H_2O activity at the onset of granulite facies metamorphism. Precambrian Research, 253, 17–25. doi: 10.1016/j.precamres.2014.06.009.

Nutman AP, Wan Y, Du L, Friend CRL, Dong C, Xie H, Wang W, Sun H, Liu D. 2011. Multistage late Neoarchaean crustal evolution of the North China Craton, eastern Hebei. Precambrian Research, 189, 43–65. doi: 10.1016/j.precamres.2011.04.005.

Peng P. 2016. Structural architecture and spatial-temporal distribution of the Archean domains in the Eastern North China Craton. In: Zhai M, Zhao Y, Zhao T(eds.), Main tectonic events and metallogeny of the North China Craton: Springer Geology. doi: 10.1007/978 –981-10–1064-4_3.

Pirajno F, Bagas L. 2008. A review of Australia's Proterozoic mineral systems and genetic models. Precambrian Research, 166, 54–80. doi: 10.1016/j.precamres.2007.05.008.

Rapp RP, Shimizu N, Norman MD, Applegate GS. 1999. Reaction between slab-derived melts and peridotite in the mantle wedge: Experimental constraints at 38 GPa. Chemical Geology, 160, 335–356. doi: 10.1016/S0009-2541(99)00106-0.

Rapp RP, Watson EB. 1995. Dehydration melting of metabasalt at 8–32 kbar: Implications for continental growth and crust-mantle recycling. Journal of Petrology, 36, 891–931. doi: 10.1093/petrology/36.4.891.

Ren LD, Geng YS, Du LL, Wang YB, Liu P, Guo JJ. 2011. Anatexis and migmatization of the Fuping Complex, North China Craton. Acta Petrologica Sinica, 27(4), 1056–1066 (in Chinese with English abstract).

Rocha BC, Moraes R, Möller A, Cioffi CR, Jercinovic MJ. 2017. Timing of anatexis and melt crystallization in the Socorro-Guaxupé Nappe, SE Brazil: Insights from trace element composition of zircon, monazite and garnet coupled to U-Pb geochronology. Lithos, 277, 337–355. doi: 10.1016/j.lithos.2016.05.020.

Shi Y, Zhao X. 2017. Early Neoarchean magmatic and paleoproterozoic metamorphic events in the northern north China Craton: SHRIMP zircon dating and Hf isotopes of Archean rocks from the Miyun area, Beijing. Acta Geologica Sinica (English edition), 91(3), 988–1002. doi: 10.1111/1755-6724.13320.

Sláma J, Kosler J, Condon DJ, Crowley JL, Gerdes A, Hanchar JM, Horstwood MSA, Morris GA, Nasdala L, Norberg N, Schaltegger U,

Schoene B, Tubrett MN, Whitehouse MJ. 2008. Plesovice zircon — A new natural reference material for U-Pb and Hf isotopic microanalysis. Chemical Geology, 249, 1–35. doi: 10.1016/j.chemgeo.2007.11.005.

Stevens G, Clemens JD, Droop GTR. 1997. Melt production during granulite-facies anatexis: Experimental data from "primitive " metasedimentary protoliths. Contributions to Mineralogy and Petrology, 128, 352–370. doi: 10.1007/s004100050314.

Stevens G, Clemens JD. 1993. Fluid-absent melting and the roles of fluids in the lithosphere: A slanted summary? Chemical Geology, 108, 1–17. doi: 10.1016/0009-2541(93)90314-9.

Sun SS, McDonough WF. 1989. Chemical and isotopic systematics of oceanic basalts: Implications for mantle composition and processes. In: Saunders AD, Norry MJ(eds.), Magmatism in the Ocean Basins. Geological Society, London, Special Publications 42, 313–345.

Swain G, Woodhouse A, Hand M, Barovich K, Shwarz M, Fanning CM. 2005. Provenance and tectonic development of the late Archaean Gawler Craton, Australia: U-Pb zircon, geochemical and Sm-Nd isotopic implications. Precambrian Research, 141, 106–136. doi: 10.1016/j.precamres.2005.08.004.

Tang M, Wang XL, Shu XJ, Wang D, Yang T, Gopon P. 2014. Hafnium isotopic heterogeneity in zircons from granitic rocks: Geochemical evaluation and modeling of "zircon effect" in crustal anatexis. Earth and Planetary Science Letters, 389, 188–199. doi: 10.1016/j.epsl.2013.12.036.

Taylor SR, Mclennan SM. 1985. The Continental Crust: Its Composition and Evolution. Oxford, Blackwell Scientific Publications, 1–312.

Vanderhaeghe O. 2009. Migmatites, granites and orogeny: Flow modes of partially-molten rocks and magmas associated with melt/solid segregation in orogenic belts. Tectonophysics, 477, 119–134. doi: 10.1016/j.tecto.2009.06.021.

Vavra G, Schmid R, Gebauer D. 1999. Internal morphology, habit and U-Th-Pb microanalysis of amphibole to granulite facies zircon: Geochronology of the Ivren Zone (Southern Alps). Contributions to Mineralogy and Petrology, 134, 380–404. doi: 10.1007/s004100050492.

Vervoort JD, Blichert-Toft J. 1999. Evolution of the depleted mantle: Hf isotope evidence from juvenile rocks through time. Geochimica et Cosmochimica Acta, 63, 533–556. doi: 10.1016/S0016-7037(98)00274-9.

Vielzeuf D, Holloway JR. 1988. Experimental determination of the fluid-absent melting relations in the pelitic system Consequences for crustal differentiation. Contributions to Mineralogy and Petrology, 98, 257–276. doi: 10.1007/BF00375178.

Vielzeuf D, Schmidt MW. 2001. Melting relations in hydrous systems revisited: Application to metapelites, metagreywackes and metabasalts. Contributions to Mineralogy and Petrology, 141, 251–267. doi: 10.1007/s004100100237.

Wan YS, Liu DY, Dong CY, Xie HQ, Kröner A, Ma MZ, Liu SJ, Xie SW, Ren P. 2015. Formation and Evolution of Archean Continental Crust of the North China Craton. In: Zhai M(ed.), Precambrian Geology of China, Springer Geology. doi: 10.1007/978 –3-662-47885–1_2.

Wan YS, Liu SJ, Xie HQ, Dong CY, Li Y, Bai WQ, Liu DY. 2018. Formation and evolution of the Archean continental crust of China: A review. China Geology, 1, 109–136. doi: 10.31035/cg2018011.

Wang W, Liu SW, Santosh M, Bai X, Li QG, Yang PT, Guo RR. 2013. Zircon U-Pb-Hf isotopes and whole-rock geochemistry of granitoid gneisses in the Jianping gneissic terrane, Western Liaoning Province: Constraints on the Neoarchean crustal evolution of the North China Craton. Precambrian Research, 224, 184–221. doi: 10.1016/j.precamres.2012.09.019.

Wang W, Liu SW, Santosh M, Deng ZB, Guo BR, Zhao Y, Zhang SH, Yang PT, Bai X, Guo RR. 2015. Late Paleoproterozoic geodynamics of the North China Craton: Geochemical and zircon U-Pb-Hf records from a volcanic suite in the Yanliao rift. Gondwana Research, 27, 300–325. doi: 10.1016/j.gr.2013.10.004.

Wei CJ, Qian JH, Zhou XW. 2014. Paleoproterozoic crustal evolution of the Hengshan-Wutai-Fuping region, North China Craton. Geoscience Frontiers, 5, 485–497. doi: 10.1016/j.gsf.2014.02.008.

Wilde SA, Valley JW, Kita NT, Cavosie AJ, Liu DY. 2008. SHRIMP U-Pb and CAMECA 1280 oxygen isotope results from ancient detrital zircons in the Caozhuang quartzite, Eastern Hebei, North China Craton: Evidence for crustal reworking 38 Ga ago. American Journal of Science, 308, 185–199. doi: 10.2475/03.2008.01.

Wu FY, Yang YH, Xie LW, Yang JH, Xu P. 2006. Hf isotopic compositions of the standard zircons and baddeleyites used in U-Pb geochronology. Chemical Geology, 234, 105–126. doi: 10.1016/j.chemgeo.2006.05.003.

Yang C, Wei C. 2017. Two phases of granulite facies metamorphism during the Neoarchean and Paleoproterozoic in the East Hebei, North China Craton: Records from mafic granulites. Precambrian Research, 301, 49–64. doi: 10.1016/j.precamres.2017.09.005.

Yang JH, Wu FY, Wilde SA, Zhao GC. 2008. Petrogenesis and geodynamics of Late Archean magmatism in eastern Hebei, eastern North China Craton: Geochronological, geochemical and Nd-Hf isotopic evidence. Precambrian Research, 167, 125–149. doi: 10.1016/j.precamres.2008.07.004.

Yang QY, Santosh M, Tsunogae T. 2016. High-grade metamorphism during Archean-Paleoproterozoic transition associated with microblock amalgamation in the North China Craton: Mineral phase equilibria and zircon geochronology. Lithos, 263, 101–121. doi: 10.1016/j.lithos.2015.11.018.

Yuan LL, Zhang XH, Zhai MG. 2015. Two episodes of Paleoproterozoic mafic intrusions from Liaoning province, North China Craton: Petrogenesis and tectonic implications. Precambrian Research, 264, 119–139. doi: 10.1016/j.precamres.2015.04.017.

Zhai M, Zhu X. 2016. Corresponding Main Metallogenic Epochs to Key Geological Events in the North China Craton: An Example for Secular Changes in the Evolving Earth. In: Zhai M, Zhao Y, Zhao T(eds.), Main tectonic events and metallogeny of the North China Craton, Springer Geology. doi: 10.1007/978–981-10–1064-4_1.

Zhai MG, Santosh M. 2011. The early Precambrian odyssey of North China Craton: A synoptic overview. Gondwana Research, 20, 6–25. doi: 10.1016/j.gr.2011.02.005.

Zhang LC, Zhai MG, Zhang XJ, Xiang P, Dai YP, Wang CL, Pirajno F. 2012. Formation age and tectonic setting of the Shirengou Neoarchean banded iron deposit in eastern Hebei Province: constraints from geochemistry and SIMS zircon U-Pb dating. Precambrian Research, 222–223, 325–338. doi: 10.1016/j.precamres.2011.09.007.

Zhao G, Sun M, Wilde SA. 2003. Correlations between the eastern block of the north China Craton and the south Indian Block of the Indian shield: An Archaean to Palaeoproterozoic link. Precambrian Research, 122(1–4), 201–233. doi: 10.1016/S0301-9268(02)00212-7.

Zhao GC, Cawood P, Lu L. 1999. Petrology and P-T history of the Wutai amphibolites: Implications for tectonic evolution of the Wutai Complex, China. Precambrian Research, 93, 181–199. doi: 10.1016/S0301-9268(98)00090-4.

Zhao GC, Sun M, Wilde SA, Li SZ. 2005. Late Archean to Paleoproterozoic evolution of the North China Craton: Key issues revisited. Precambrian Research, 136, 177–202. doi: 10.1016/j.precamres.2004.10.002.

Zhao GC, Wilde SA, Cawood PA, Lu LZ. 1998. Thermal evolution of Archean basement rocks from the eastern part of the North China Craton and its bearing on tectonic setting. International Geology Review, 40, 706–721. doi: 10.1080/00206819809465233.

Zhao GC, Wilde SA, Cawood PA, Sun M. 2001. Archean blocks and their boundaries in the North China Craton: Lithological, geochemical, structural and P-T path constraints and tectonic evolution. Precambrian Research, 107, 45–73. doi: 10.1016/S0301-9268(00)00154-6.

Zheng YF, Hermann J. 2014. Geochemistry of continental subduction-zone fluids. Earth Planets Space, 66, 93. doi: 10.1186/1880-5981-66-93.

Zulbati F, Harley SL. 2007. Late Archaean granulite facies metamorphism in the Vestfold Hills, East Antarctica. Lithos, 93, 39–67. doi: 10.1016/j.lithos.2006.04.004.